Available online at www.sciencedirect.com

ScienceDirect

Mendeleev Commun., 2019, **29**, 269–272

Mendeleev Communications

Hierarchical structure of SERS substrates possessing the silver ring morphology

Anna A. Semenova,[a] Sergey V. Savilov,[b] Alexander E. Baranchikov,[c] Vladimir K. Ivanov[a,c] and Eugene A. Goodilin*[a,b,c]

[a] *Department of Materials Science, M. V. Lomonosov Moscow State University, 119991 Moscow, Russian Federation. Fax: +7 495 939 0998; e-mail: goodilin@yandex.ru*
[b] *Department of Chemistry, M. V. Lomonosov Moscow State University, 119991 Moscow, Russian Federation*
[c] *N. S. Kurnakov Institute of General and Inorganic Chemistry, Russian Academy Sciences, 119991 Moscow, Russian Federation*

DOI: 10.1016/j.mencom.2019.05.009

Nanostructured silver coatings for surface-enhanced Raman spectroscopy possessing a hierarchic ring morphology were prepared *via* the superficial decomposition of ultrasonic mist of aqueous diamminesilver(I) hydroxide free of reducing agents and non-volatile pollutants. These materials are explored in terms of their processing, morphology, and functional SERS applications.

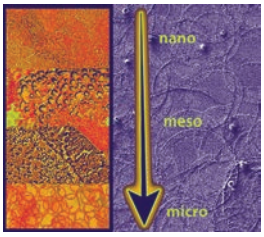

Surface-enhanced Raman spectroscopy (SERS)[1–4] conquests quickly the niche of chemical, ecological and biomedical diagnostics,[5–9] however these efforts still demand the development of new SERS active materials.[8–11] The preparation route of SERS substrates suggested in this work is simple[12–14] and can be easily reproduced in common laboratory practice using readily available reagents. During the deposition process, ammonia complex solution of silver(I) hydroxide was nebulized into mist, and the obtained droplets (1–5 μm) were streamed onto clean glasses under mild conditions (270–290 °C) resulting in SERS-active substrates containing nanostructured silver ring layers.‡ Aqueous ammonia forms a relatively stable silver hydroxide complex;[11] however, its decomposition starts upon heating so the complex releasing NH_3 evolved into the surrounding atmosphere and thus giving some amount of Ag^+. The latter can be reduced either by OH^- or NH_3 followed by a nucleation of silver nanoparticles (AgNPs). Note that NH_3 is a stronger reducing agent as compared to OH^- since the standard potential of the pair N_2/NH_3 is –0.74 V. Thus, the overall potential of reaction $3Ag^+ + NH_3 + 3OH^- = 3Ag + {}^1/_2N_2 + 3H_2O$ is quite high (E^0 = +1.39 V). In this process, there are no reagents exhibiting a complicated behavior, no complicated reaction pathways, and no critical dependence on a reagent mixing order. This allowed us to believe that this robust approach would be experimentally suitable for the AgNPs preparation.

We have found that an effective and scalable way to prepare AgNPs based on diamminesilver(I) hydroxide is uniquely related to thermal decomposition of ultrasonic mist of this precursor, *i.e.*, this deposits pure nanostructured silver coatings (Figure 1). Quick supersaturation growth and relaxation that favor a smaller size of AgNPs were provided by either fast heat and mass transfer due to a large surface area of the mist or an abrupt temperature jump, when the mist reaches a hot zone onto the substrate surface. Silver complex decomposition occurs in droplets as in microreactors; the latter also provide a constraint growth of AgNPs. Each droplet suffers a thermal shock followed by a decrease in ammonia concentration and partial water evaporation at the beginning. The absence of insoluble or precipitating impurities makes the procedure suitable for nanostructured silver deposition onto various substrates.

According to TEM and electron diffraction (ED) data, preparation conditions of the substrates, such as the temperature and spraying time, play an important role as evident for the substrates preheated up to 60 °C and kept under an aerosol stream for 40 min [Figure 1(*a*),(*b*)], and for the same deposition time but at a constant temperature of 270 °C [Figure 1(*c*),(*d*)]. The reason was that either silver(I) oxide formed as an intermediate at lowered temperatures or primary silver particles were fed and then grew by the incoming portions of nutrient silver(I) complex. Lowered temperatures resulted in rings consisting of semi-decomposed silver(I) oxide [see Figure 1(*a*),(*b*)]. Microscopically, their walls possess a structure composed of silver(I) oxide with elongated

† $AgNO_3$, NaOH, NH_4OH (aq., 30%), and Rhodamine 6G (Rh6G) were of high purity grade. Ultra-pure water with resistivity *ca.* 18 MΩ cm (Milli-Q, Millipore) was used. Aqueous sodium hydroxide (0.1 M) was added dropwise to a freshly prepared silver nitrate solution (10 mM) until the completed precipitation of a black-brown silver(I) oxide. The oxide was thoroughly washed with deionized water and dissolved in a twofold molar excess of aqueous ammonia (10%) to give 0.0125 M solution of silver(I) complex. The obtained transparent silver complex solution was filtered through Millex-LCR syringe driven filter units (Millipore, pores of 0.45 mm).

‡ The obtained materials were characterized by the transmission and scanning electron microscopy (TEM and SEM, respectively) using a LEO912 AB OMEGA (Carl Zeiss) and NVision 40 (Carl Zeiss) electron microscopes, and by X-ray powder diffraction (XRD) using a Rigaku D/MAX 2500 diffractometer (Japan) equipped with a rotating copper anode (CuKα irradiation, 2θ range of 5–80°, step of 0.02°). Raman and SERS experiments were performed using an InVia Raman microscope (Renishaw, UK) equipped with an argon laser (20 mW, 514 nm) and power neutral density filter (1–10%). All the spectra were collected by 20-fold objective lens for acquisition time of 10–120 s; a silicon wafer was used for preliminary calibration.

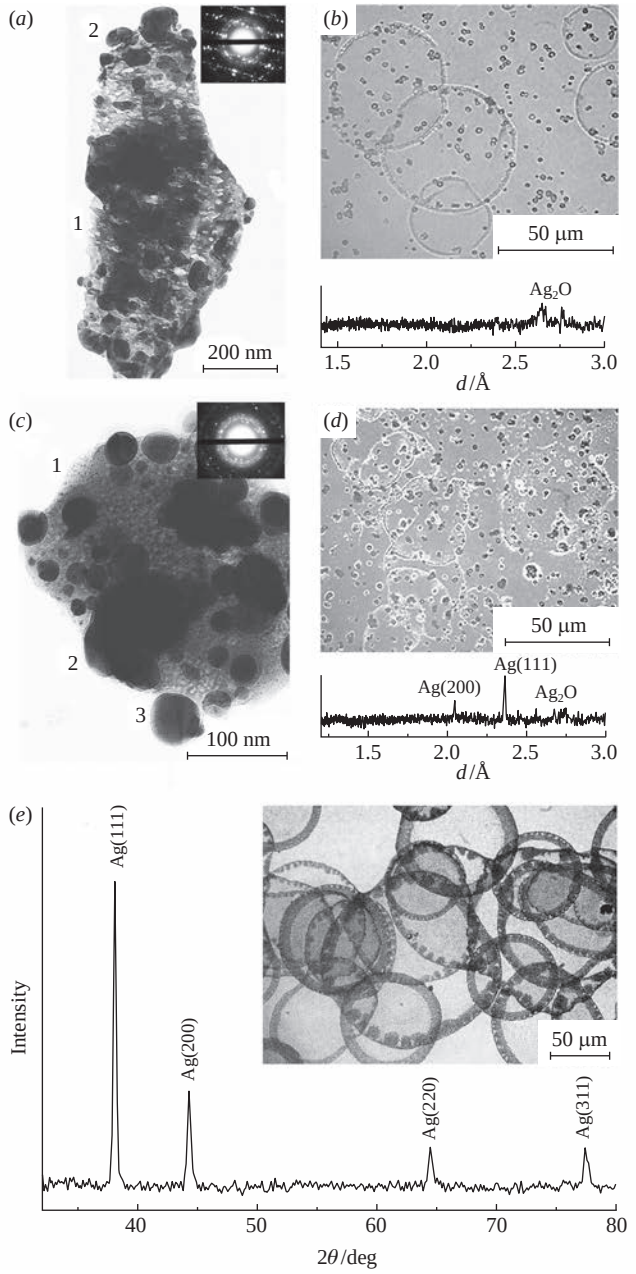

Figure 1 Phase assembling in the deposition process of silver ring nanostructures. Typical (*a*),(*c*) TEM and (*b*),(*d*) optical images of silver ring fragments formed under different conditions. The insets show electron diffraction patterns for the samples. The porous structure of Ag_2O (1) and incorporated metallic nanoparticles (2, 3) are denoted, and XRD patterns are given below the pictures (*b*) and (*d*). (*e*) Typical XRD data on the final silver ring substrates and transmission optical images of the ring structures (shown in the inset).

and partly co-oriented pores coexisting with rather small (3–30 nm) nanoparticles of metallic silver [see Figure 1(*a*)]. An ED pattern shows at least two phases including silver and silver(I) oxide. Higher temperatures resulted in a porous silver structure ('silver sponge') with embedded silver grains [see Figure 1(*c*),(*d*)]. Macroscopically, XRD of the nanostructures correspond to the structural features detected microscopically. In particular, a cubic modification of metallic silver was found from the XRD data for the sample produced at mild temperatures applied to the substrates, while an Ag/Ag_2O mixture or even Ag_2O were observed otherwise (see Figure 1).

In terms of the general chemistry, a thermal treatment of ultrasonic mists of the diamminesilver(I) hydroxide complex leads to its irreversible decomposition and solvent evaporation. The products of this transformation include nanostructured silver

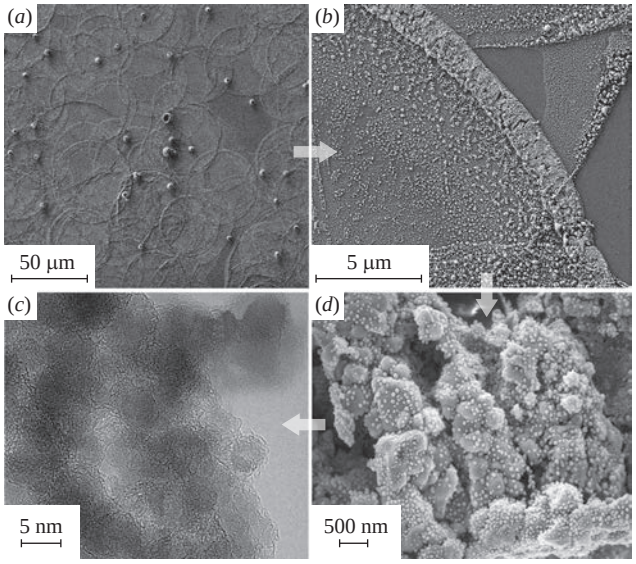

Figure 2 Hierarchical structure of nanostructured ring coatings: (*a*) general view (SEM) of intersecting silver rings, (*b*) SEM view of silver ring walls, (*c*) SEM graph of silver sponge of the ring rims, and (*d*) high resolution TEM image of the silver sponge consisting of silver nanoparticles and empty channels.

particles, water, ammonia, and oxygen. Quenching of such products yields nanostructured particles and their aggregates formed in a shock manner since the whole transformation occurs for few seconds upon heating and contacting with the hot surface of substrates. The silver ring structures are formed at moderate temperatures of 200–250 °C due to the deposition of mist droplets onto a preheated substrate (Figures 2 and 3). The coatings consist of overlapped silver rings of a complex morphology originated from decomposition of micron-sized droplets of ultrasonic mist of silver(I) solution. Usually, silver deposition gives intersecting circles of 30–100 μm in diameter. This value is several times larger than the expected size of 1–10 μm of the falling mist droplets, since the liquid from the droplets spreads laterally over the substrate. The solvent evaporation increases the concentration of silver complex, and metallic silver then resides on rims of the

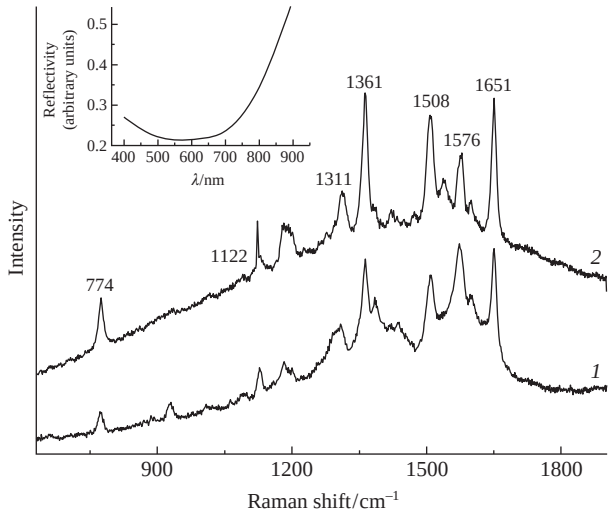

Figure 3 Typical SERS spectra of the model analyte (Rh6G dye) measured at 5% of laser power, recording for 10 s, Rh6G concentration of 10^{-8} mol dm^{-3}, using the nanostructured ring substrates (*1*) *vs*. dried nanoparticles (size of 20–30 nm) on a glass plate prepared according to the Leopold–Lendl method, recorded at 1% of laser power, acquisition time of 10 s, Rh6G concentration of 10^{-7} mol dm^{-3} (*2*). The inset shows a reflectivity spectrum of the nanostructured surface demonstrating a wide plasmonic band of the substrate.

spreading circles producing walls of silver rings. The thickness of walls was found to be typically within 1–3 μm, while the residual part was covered with randomly distributed silver nanoclusters gradually increasing in sizes from 10–20 nm in the centers of the circles to about 100 nm in the wall vicinity. The nanoclusters increase the role of capillary forces, so more droplets are stacked onto the surface and boil, while an increased sputtering time leads to rough and porous layers (see Figure 2).

This deposition mode possesses several advantages in terms of formation of SERS-active structures for promising applications: (i) silver micro- and nanostructures are immobilized onto a substrate and form a rather stable metallic film on cheap materials like glass, (ii) there is no need to filter or separate the nanoparticles, (iii) the nanostructure consists of porous silver sponge, and (iv) the temperatures are high enough for the one-step formation of pure metallic silver nanostructured layer without any remaining byproducts.

A closer look at the microstructure of the silver coated substrates (see Figure 2) revealed that all of them consist of overlapping silver rings of a complex morphology originated from decomposition of micrometer-sized droplets of ultrasonic mist of silver(I) solution.[§]

Most of the circles form groups or long chains until the surface becomes quite uniformly covered with stochastically intersecting silver rings. These grouping effect cannot be simply explained by a probability of striking the surface by the incoming droplets, since the stream of ultrasonic mist exceeded the substrate size, and the droplets had to be mixed more or less uniformly in the mist thus providing an equal superficial density of their meeting points with the surface. We have experimentally observed a small induction time (~5 min) prior to the visual coverage of substrates with the first traces of silver. This should mean that the actual sequence of events was complex and, at least, there was a pinning effect of incoming droplets onto the already formed silver rings. The final result of droplet evolution was the formation of heavily interlacing silver craters. Adhesion and wetting were drastically increased upon the formation of first silver rings making the surface rough and providing seeds for the further nucleation of silver from mist droplets in the intersecting areas of the rings. Additional features like rim widening on a group of primary rings, chain formation, ring elongation, and rim polygonization are the consequence of different wetting properties of the substrate surface changing with time. Dewetting of residual liquid film resulted in silver clusters inside the rings. Importantly, the silver ring formation process onto the substrates was accompanied by nanostructuring. When silver ring forms, large and smaller gaps appear in the region of rims and this gives random blocks (‘bricks’ of the wall) of 200–500 nm (see Figure 2). The bricks and walls are composed of nanometer-sized interconnected silver particles because an every act of droplet transformation on the substrate gives newborn AgNPs of a very small size (several nanometers, see Figure 2). Later, these nanoparticles grow, join each other, and form channels making the observed high porosity of the silver walls possible. Instant capillary transport of nutrient solution to the top of walls through the channels leads to growth of silver grains (size of 20–40 nm) covering the bricks. A thorough inspection allowed us to assume that dissolution of neighbor smaller nanoparticles of the matrix supplies further growth of larger ‘sesame seeds’. All the elements of this hierarchical structure are conductive and that provides various opportunities for the plasmon coupling.

In a full agreement with the XRD data (see Figure 1), a number of plasmonic bands appear for these nanostructured substrates with pure silver (see Figure 3, inset) thus forming a very wide light absorption band with a long tail towards larger wavelengths because of the hierarchic nature of the coatings described above. This allowed us to use most of popular lasers with 514, 532, 633 and 785 nm wavelengths to agitate plasmons and plasmon-polaritons, while much narrower peaks were observed, *e.g.*, for separated nanoparticles and sols[1–4] making them less effective in terms of the enhancement of Raman signals for particular lasers. The substrates demonstrated excellent plasmonic behavior exceeding the same parameter for AgNPs sols immediately after their fast and easy preparation without any application of an additional treatment (see Figure 3).[¶] Thermal decomposition of diamminesilver(I) hydroxide solutions enables preparing nanostructured silver materials with an uniformly low background signal and the latter becomes possible due to the combination of highly nonequilibrium preparation conditions guaranteeing a small size of forming nanoparticles and their aggregates and also a high enough temperatures preventing physical adsorption and chemisorption of byproducts. Moreover, aerosol deposition is a scalable method suitable for the preparation of either nanoparticles of a complex shape or planar nanostructures with a large number of ‘hot spots’.[14]

As soon as molecules inside living cells are considered, no physical contact between nanoparticles and the analyte molecules occurs. Obviously, ‘hot spot’ and the charge transfer enhancement vanish in SERS of living cells since they require a direct contact between the analyte molecules and nanostructures.[13,14] Therefore, the remaining electromagnetic field enhancement becomes a dominant mechanism. This enhancement depends strongly on superficial nanostructuring, so the morphology of the nanostructured ring substrates allows this mechanism to work out. Thus, this preparation technique seems to be appropriate as a method of choice for the obtaining of functional components for new SERS devices. The observed microstructural features are responsible for successful application of the substrates for a large variety of objects, including dyes, oil contaminants, living cells and their compartments.[10,11,13,14]

In conclusion, a new simple preparation method for the SERS-active nanostructured coatings on suitable surfaces becomes readily available *via* utilization of silver(I) oxide complexes free of special reducing agents or anionic pollutants. The substrates produced under mild conditions demonstrate a unique hierarchic morphology originated of ultrasonic droplet decomposition and overlay of their collapsing zones. The preparation technique of nanostructured ring substrates looks to be a promising method for the production of functional components for new SERS devices. The fabricated substrates are a remarkable example of an original scalable material suitable for SERS analyses, which is easy-to-produce and stable[10,11] thus ensuring a better

[§] Such a complicated circular morphology of the nanostructured silver coatings might be caused by the ‘coffee ring’ effect involving various processes, in particular, the contact-line motion, directed assembly, flow instabilities, and the formation of a surface-skin.[14] Indeed, if a drop of liquid dries on a solid surface forming nanoparticles, the latter would be deposited in a ring-like manner. During the drying process, drop edges become pinned to the substrate, and capillary flow outward from the centre of the drop brings suspended particles to the edge as the evaporation is proceeding. The particles are concentrated along the original drop edge. As soon as the formed nanoparticles are moved to the rim, their local attractions lead to the formation of packed structures near the rim. The structures prevent the particles from reaching the droplet edge and make the deposition more uniform. The complexity of the ‘coffee ring’ scenario yields the observed unusual silver ring structures for all the ring substrates.

[¶] In this case, Leopold–Landl AgNPs[15] demonstrated a high background contribution of luminescence at higher Rh6G concentrations or higher laser power, while the selected Rh6G concentration of 10^{-8} M gave an inappropriate signal-to-noise ratio.

reproducibility and less toxicity, and promoting their SERS applications in biology and medicine.

This work was supported in its instrumental part by the M. V. Lomonosov Moscow State University Program of Development. EAG was supported by the Russian Science Foundaton (grant no. 14-13-00871), and AAS was supported by the Grant of the President of the Russian Federation for the governmental support of young scientists (grant no. MK-1146.2017.3). The authors are grateful to A. V. Egorov, N. A. Brazhe, and S. M. Novikov for their assistance and fruitful discussions.

References

1 R. A. Alvarez-Puebla and L. M. Liz-Marzán, *Small*, 2010, **6**, 604.
2 Z. Wang, S. Pan, T. D. Krauss, H. Du and L. J. Rothberg, *Proc. Natl. Acad. Sci. USA*, 2003, **100**, 8638.
3 J. Fang, S. Liu and Z. Li, *Biomaterials*, 2011, **32**, 4877.
4 J. N. Anker, W. P. Hall, O. Lyandres, N. C. Shan, J. Zhao and P. V. Van Duyne, *Nat. Mater*., 2008, **7**, 442.
5 X. Wang, Y. Li, H. Wang, Q. Fu, J. Peng, Y. Wang, J. Du, Y. Zhou and L. Zhan, *Biosens. Bioelectron*., 2010, **26**, 404.
6 A. März, B. Mönch, P. Rösch, M. Kiehntopf, T. Henkel and J. Popp, *Anal. Bioanal. Chem*., 2011, **400**, 2755.
7 J. Kneipp, H. Kneipp, B. Wittig and K. Kneipp, *Nano Lett*., 2007, **7**, 2819.
8 R. M. Jarvis and R. Goodacre, *Chem. Soc. Rev*., 2008, **37**, 931.
9 T. A. Taton and C.A. Mirkin, *Science*, 2000, **289**, 1757.
10 O. E. Eremina, A. A. Semenova, E. A. Sergeeva, N. A. Brazhe, G. V. Maksimov, T. N. Shekhovtsova, E. A. Goodilin and I. A. Veselova, *Russ. Chem. Rev*., 2018, **87**, 741.
11 A. A. Semenova, A. P. Semenov, E. A. Gudilina, G. T. Sinyukova, N. A. Brazhe, G. V. Maksimov and E. A. Goodilin, *Mendeleev Commun*., 2016, **26**, 177.
12 A. S. Sarycheva, N. A. Brazhe, A. A. Baizhumanov, E. I. Nikelshparg, A. A. Semenova, A. V. Garshev, A. E. Baranchikov, V. K. Ivanov, G. V. Maksimov, O. Sosnovtseva and E. A. Goodilin, *J. Mater. Chem. B*, 2016, **4**, 539.
13 N. A. Brazhe, A. B. Evlyukhin, E. A. Goodilin, A. A. Semenova, S. M. Novikov, S. I. Bozhevolnyi, B. N. Chichkov, A. S. Sarycheva, A. A. Baizhumanov, E. I. Nikelshparg, L. I. Deev, E. G. Maksimov, G. V. Maksimov and O. Sosnovtseva, *Sci. Rep*., 2015, **5**, srep13793.
14 A. A. Semenova, E. A. Goodilin, N. A. Brazhe, V. K. Ivanov, A. E. Baranchikov, V. A. Lebedev, A. E. Goldt, O. V. Sosnovtseva, S. V. Savilov, A. V. Egorov, A. R. Brazhe, E. Y. Parshina, O. G. Luneva, G. V. Maksimov and Y. D. Tretyakov, *J. Mater. Chem*., 2012, **22**, 24530.
15 N. Leopold and B. Lendl, *J. Phys. Chem. B*, 2003, **107**, 5723.

Received: 7th December 2018; Com. 18/5762